In fact, although the spectrum of such junctions depends on the difference of the phases of the order parameter φ, nonetheless at low transparency ($V \to \infty$) this dependence is weak, so that the level smearing in this case is also small (including also in strong magnetic fields). It can consequently be assumed that in SNINS systems the magnetic field does not upset the discrete character of the excitation spectrum even at rather appreciable dimensions of the system (in the y direction), whereas in SNS junctions in a strong magnetic field it is utterly meaningless to speak of discrete excitation-energy levels, and the spectrum in this case is continuous. These conclusions can be reconciled completely with experiment. We have constructed also a microscopic theory of the stationary Josephson current in SNINS junctions. The magnitude and quite unique temperature dependence of this current, which are governed by the presence of a phase-coherent spectrum of discrete states in the system, is strongly influenced also by the position of the insulating barrier inside the normal-metal layer.

The noted singularities of the behavior of SNINS systems can in all probability be used also for further experimental study of the proximity effect.

[1]A. F. Andreev, Zh. Eksp. Teor. Fiz. **46**, 1823 (1974); **49**, 655 (1965) [Sov. Phys. JETP **19**, 1228 (1974); **22**, 455 (1966)].
[2]I. O. Kulik, Zh. Eksp. Teor. Fiz. **57**, 1745 (1969) [Sov. Phys. JETP **30**, 944 (1969)].
[3]C. Ishii, Prog. Theor. Phys. **44**, 1525 (1970).
[4]A. V. Svidzinskiĭ, T. N. Antsygina, and E. N. Bratus', Zh. Eksp. Teor. Fiz. **61**, 1612 (1971) [Sov. Phys. JETP **34**, 860 (1971)].
[5]J. Bardeen and J. L. Johnson, Phys. Rev. **5B**, 72 (1972).
[6]I. O. Kulik, Weak Superconductivity, Preprint, Inst. Metal Phys. USSR Acad. Sci., Sverdlovsk, 1973.
[7]V. Ambegaokar and A. Baratoff, Phys. Rev. Lett. **10**, 486 (1963); **11**, 104 (1963).
[8]N. N. Bogolyubov, Usp. Fiz. Nauk **67**, 549 (1959) [Sov. Phys. Usp. **1**, 236 (1959)].
[9]P. de Gennes, Superconductivity of Metals and Alloys, Benjamin, 1966.
[10]A. I. Bezuglyĭ, I. O. Kulik, and Yu. N. Mitsai, Fiz. Nizk. Temp. **1**, 57 (1975) [Sov. J. Low Temp. Phys. **1**, 27 (1975)].
[11]V. P. Galaĭko, Zh. Eksp. Teor. Fiz. **57**, 941 (1969) [Sov. Phys. JETP **30**, 514 (1970)].
[12]V. P. Galaĭko and E. V. Bezuglyĭ, Zh. Eksp. Teor. Fiz. **60**, 1471 (1971) [Sov. Phys. JETP **33**, 796 (1971)].
[13]G. A. Gogadze and I. O. Kulik, Zh. Eksp. Teor. Fiz. **60**, 1819 (1971) [Sov. Phys. JETP **33**, 984 (1971)].
[14]A. A. Abrikosov, L. P. Gor'kov, and I. E. Dzyaloshinskiĭ, Metody kvantovoi teorii polya v statisticheskoĭ fizike (Quantum Field-Theoretical Methods in Statistical Physics), Fizmatgiz, 1962 [Pergamon, 1965].
[15]I. O. Kulik and I. K. Yanson, Éffekt Dzhozefsona v sverkhprovodyashchikh tunnel'nykh strukturakh (Josephson Effect in Superconducting Tunnel Structures), Nauka, 1970.
[16]I. O. Kulik and Yu. N. Mitsai, Fiz. Nizk. Temp. **1**, 906 (1975) [Sov. J. Low Temp. Phys. **1**, 434 (1975)].

Translated by J. G. Adashko

Anisotropy of the magneto-optical properties of cobalt single crystals

E. A. Gan'shina, G. S. Krinchik, L. S. Mironova, and A. S. Tablin

Moscow State University

(Submitted 18 July 1979)
Zh. Eksp. Teor. Fiz. **78**, 733–740 (February 1980)

The magneto-optical spectra of cobalt single crystals were investigated in the energy region 0.2–3.35 eV. Anisotropy of the frequency spectra of the equatorial Kerr effect was observed in the case of magnetization along different crystallographic directions. The off-diagonal components of the dielectric tensor are calculated. The observed anomalies are identified with definite interband transitions when account is taken of the selection rules for a hexagonal crystal. It is shown that the magneto-optical spectra for cobalt agree best with the band structure proposed for ferromagnetic cobalt by Batallan and co-workers.

PACS numbers: 78.20.Ls, 71.25.Pi

INTRODUCTION

Many physical properties of ferromagnetic 3*d* metals and alloys have by now been explained within the framework of the magnetism theory of Slater, Stoner, and Wohlfarth by invoking the concepts of single-electron band theory. Cobalt, just as nickel, is a typical band ferromagnet. Calculations of the electronic structure of cobalt were reported in a number of theoretical papers.[1-8]

Connoly[1] was the first to publish data on the band structure of cobalt in individual high-symmetry points of the Brillouin zone. The calculations were made by the augmented plane-wave method with optimized spin-dependent potential. The exchange splitting in his model was assumed to be 2 eV. Wakoh and Yamashita[2] later calculated the energy bands and the Fermi surface, using the Korringa–Kohn–Rostoker (KKR) method with constant exchange splitting ($\Delta E_{dd} = 1.73$ eV). Ishida[3] calculated the band structure of hexagonal cobalt by using amodified Muller interpolation scheme. None of the presented structures provided a satisfactory description of the experimental data obtained later on the

0038-5646/80/020369-05$02.40

topology of the Fermi surface in cobalt single crystals[4] and the photoemission effects.[5] Batallan and co-workers[6] performed new calculations of the band structure of cobalt by the KKR method with allowance for the spin-orbit interaction. The obtained topology of the Fermi surface was in good agreement with experiments on the de Haas–van Alphen effect, and the calculated state-density curve explained the available photoemission data, while the exchange splitting was equal to 1.39 eV.

Singal and Das[7] were the first to calculate the electronic structure of cobalt using a nonlocal Hartree-Fock exchange potential, which took exact account of the influence of the correlation effects on the single-electron energy levels. In their model they also succeeded in adequately explaining the observed magnetic properties of cobalt (the magnetization and the topology of the Fermi surface). The exchange splitting of the $3d$ bands obtained in their calculations equals 3.9 eV. A theoretical estimate of the most probable exchange splitting of the $3d$ bands, carried out by Wohlfarth[8] on the basis of the theory of band magnetism, yields for ΔE_{dd} a value of 1.05 eV.

Thus, the value of ΔE_{dd} and the relative position of the s, p, and d bands differ significantly in the existing models of the electronic structure of cobalt.

Experimental information on these values can be obtained by studying the optical and magneto-optical spectra. Many studies of the optical properties of cobalt[9-12] have shown that in cobalt the interband transitions begin with an energy on the order of 0.2 eV, and an intense absorption band exists in the region of 0.85 eV. In the study of the magneto-optical properties of a polycrystal, an anomaly was observed in the region 0.7–1.0 eV.[13]

To our knowledge, no magneto-optical investigations of single-crystal cobalts were made so far. It was therefore of interest to study the magneto-optical properties in the infrared and visible regions of the spectrum, for the purpose of determining the details of the electronic structure of Co, as was done in the study of the magneto-optical spectra of nickel.[14]

EXPERIMENTAL RESULTS

We investigated in the present study the equatorial Kerr effect (EKE) in the region of light-photon energy 0.2–3.35 eV, on single-crystal samples of ferromagnetic Co. The measurements were made by a dynamic method, and the schematic diagram of the setup and the details of the method are described in Ref. 15. We note only that the sample magnetization was reversed in a field of 14 kOe, sufficient to magnetize the sample to saturation in any crystallographic direction.

The Co samples were cut in two cyrstallographic planes, (0001) and (1010), from a single-crystal ingot grown by the (Bridgman) method of directional crystallization. The plane of the sample coincided with the chosen crystallographic plane accurate to 3°, as monitored by plotting the reflection Laue patterns. Prior to the measurement, the samples were mechanically and electrolytically polished.

Figure 1 shows the EKE dispersion curves measured for single-crystal Co at a light incidence angle $\varphi = 70°$ for different orientations of the magnetization vector relative to the easy magnetization axis [0001] (the C axis).

Figure 2 shows the analogous curves for a light-incidence angle 80°. From a comparison of these curves, as well as of the curves for a sample cut in the basal plane (Fig. 3), it is seen that the magneto-optical properties of ferromagnetic cobalt are highly anisotropic. All the curves have a deep minimum in the region 0.3–0.35 eV, as well as a second sufficiently well pronounced minimum in the region 0.8–1.1 eV. For a polycrystalline sample, this anomaly was observed in the form of a step and revealed a fine structure only in low-temperature measurements.[13] In the EKE measurements, the maximum and minimum of the region of this anomaly shift to the low-energy region on going from one axis (H ∥ C) to another (H ⊥ C). In the 1.5 eV region, all the curves have a broad maximum, just as in the case of the polycrystalline sample. The anisotropic behavior of the plots of the EKE against $\hbar\omega$ can be noted also in the region 2.0–3.0 eV.

From the measured values of the EKE at two light-incidence angles we calculated the real and imaginary parts of the off-diagonal components of the dielectric tensor. Since hexagonal cobalt is from the optical point of view a uniaxial crystal, to find the magneto-optical constants of cobalt we used the dielectric tensor in the form

$$\varepsilon = \begin{vmatrix} \varepsilon_x - i\varepsilon' & 0 \\ i\varepsilon' & \varepsilon_y \\ 0 & 0 \end{vmatrix} \quad \begin{matrix} 0 \\ 0 \\ \varepsilon_z \end{matrix}, \tag{1}$$

where $\varepsilon' = \varepsilon_1' - i\varepsilon_2'$ is the off-diagonal component of the tensor ε and determines the magneto-optical properties of the cobalt. In place of the diagonal components ε_i $(i = x, y, z)$ we substituted the values of $\varepsilon_\parallel$ or $\varepsilon_\perp$, depending on the orientation of the plane of the sample to the magnetization direction relative to the optical axis.

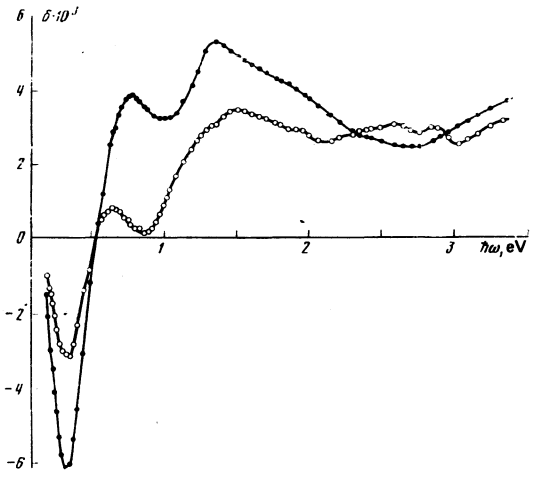

FIG. 1. EKE in a Co single crystal cut in the [010$\bar{1}$] plane for $\varphi = 70°$ at various orientations of the magnetization vector relative to the easy magnetization axis (0001): ●– H ∥ C, ○– H ⊥ C.

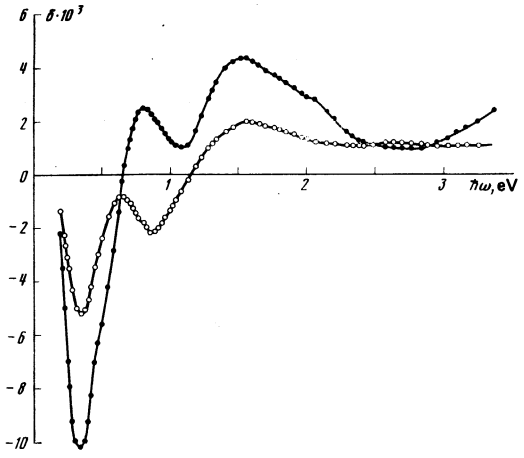

FIG. 2. EKE in a Co single crystal cut in the [010$\bar{1}$] plane for $\varphi = 80°$ at various orientations of the magnetization vector relative to the easy magnetization axis C: • – $H \| C$, ○ – $H \perp C$.

A diagram of the incidence of the light on the sample and the orientation of the axes are shown in Fig. 4.

Using the tensor (1) in the solution of Maxwell's equation, we obtain for the EKE in a uniaxial crystal the relation

$$\delta = \varepsilon_2' F - \varepsilon_1' G, \tag{2}$$

where

$$F = 2\frac{L \sin 2\varphi}{L^2 + M^2}, \quad G = 2\frac{M \sin 2\varphi}{L^2 + M^2},$$

$$L = a_1 - \sin^2\varphi - (a_1 a_2 - b_1 b_2)\cos^2\varphi,$$

$$M = b_1 - (a_1 b_2 + a_2 b_1)\cos^2\varphi, \quad \varepsilon_i = \varepsilon_{1i} - i\varepsilon_{2i},$$

$$a_1 = \varepsilon_{1y}, \quad a_2 = \varepsilon_{1x}, \quad b_1 = \varepsilon_{2y}, \quad b_2 = \varepsilon_{2x}.$$

The values of ε_1' and ε_2' for different orientations of the vectors E and H relative to the optical axes were calculated from the values of $\delta(\hbar\omega)$ at two light-incidence angles, using the formulas

$$\varepsilon_1' = \frac{\delta_1 F_2 - \delta_2 F_1}{F_1 G_2 - G_1 F_2}, \quad \varepsilon_2' = \frac{\delta_1 G_2 - \delta_2 G_1}{F_1 G_2 - G_1 F_2}. \tag{3}$$

The optical constants for single-crystal Co were taken from Ref. 9.

Figures 5 and 6 show the dispersion curves $\varepsilon_1'(\hbar\omega)^2$ and $\varepsilon_2'(\hbar\omega)^2$ at various orientations of the magnetization vector relative to the crystallographic axes.

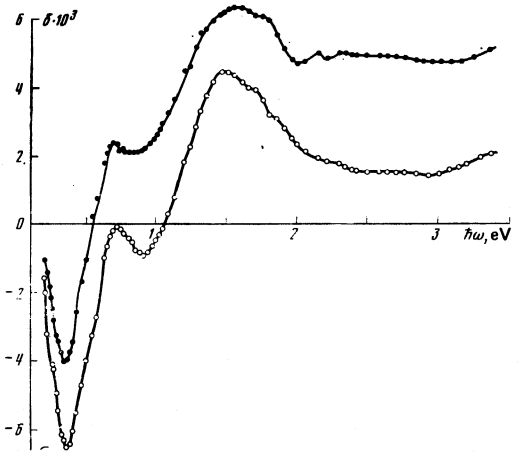

FIG. 3. EKE for Co single crystal cut in the basal plane at two light-incidence angles: • – $\varphi = 70°$, ○ – $\varphi = 80°$.

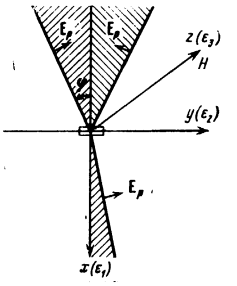

FIG. 4. Diagram of the incidence of light on the sample and orientation of the axes: the light-incidence plane is xy, the sample plane is yz, the external field $H \| z$, and $\mathbf{E}_p$ is the effective electric vector of the light wave.

DISCUSSION OF RESULTS

The value of ε_2' is determined, just as in optics, by two contributions: intraband and interband. It was estimated[12] that for polycrystalline Co the contribution of the free carriers to the optical constant becomes negligible already in the infrared region, where it still is 50% at $\lambda = 8$ μm, but only 4% at $\lambda = 2$ μm.

According to the estimate in Ref. 16, the contribution of the free carriers to the magneto-optical properties is constant and small, ensuring only a small shift of the entire ε_2' curve. The behavior of the magneto-optical properties of Co in the near infrared and visible regions can therefore be regarded as governed by the interband transitions. For direct interband transitions, $\varepsilon_2'(\hbar\omega)^2$ is proportional to the interband state density

$$\varepsilon_2'(\hbar\omega)^2 \sim \sum_{mn} f_{mn}\frac{dN}{dE_{mn}} = \frac{1}{\Omega}\sum_{mn} f_{mn}\int \frac{dS}{\nabla_k(E_m - E_n)},$$

where f_{mn} is the interband oscillator strength, S is one of the equal-energy surfaces defined by the condition $\hbar\omega = E_m(k) - E_n(k)$, and the singularities on the $\varepsilon_2'(\hbar\omega)^2$ curves are connected with the singularities in the interband state density. We shall analyze the behavior of the

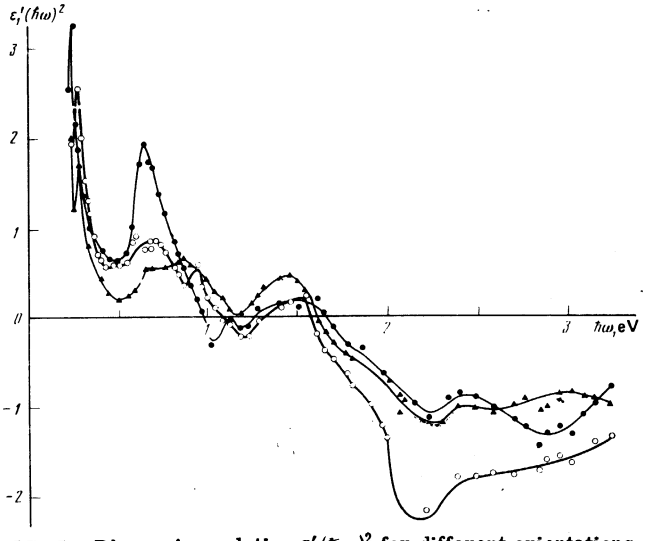

FIG. 5. Dispersion relation $\varepsilon_1'(\hbar\omega)^2$ for different orientations of the magnetization vector relative to the crystallographic axes: • – $H \| C$, ▲ – $H \perp C$, ○ – basal plane.

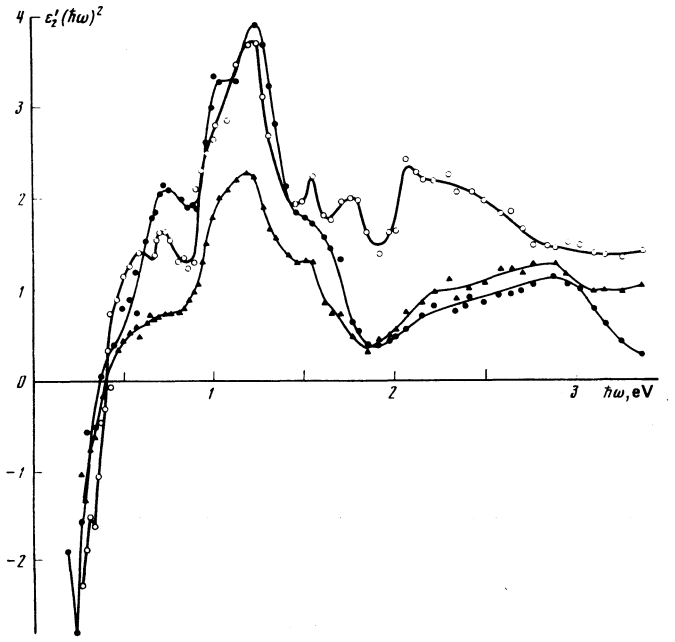

FIG. 6. Dispersion relations $\varepsilon_2'(\hbar\omega)^2$ at various orientations of the magnetization vector relative to the crystallographic axes: – H‖C, ▲ – H⊥C, ○ – basal plane.

$\varepsilon_2'(\hbar\omega)^2$ curves on the basis of the existing data on the electronic band structure of ferromagnetic cobalt.

In the picture of the electronic band structure of cobalt, obtained by Batallan and co-workers (see Fig. 2 in Ref. 6), the lowest-energy transitions are located in the subband with spin ↑ in the region of the point Γ where, according to measurements of the de Haas–van Alphen effect, is located a neck similar to the neck at the point L of Ni.[17] It can be noted that in the earlier band calculations (see, e.g., Ref. 2), these necks were absent and the low-energy transitions in the subband with spin ↑ vanished. This was due to the overestimate of the exchange splitting (1.71 eV). When this quantity is decreased to 1.1–1.3 eV, necks appear in the point Γ, for the electron spectrum obtained by Wakoh and Yamashita, as well as the low-energy transitions needed to explain the magneto-optical properties of cobalt. In the model of Singal and Das, owing to the excessively large distance between the s and d bands, there are likewise no low-energy transitions in the subband with spin ↑, although necks do exist at the point Γ.

Thus, according to the Batallon model, the negative peak on the $\delta(\hbar\omega)$ curves and the values of $\varepsilon_2'(\hbar\omega)^2$ in the region 0.2–0.3 eV are attributed by us to the existence of direct interband transitions in the vicinity of the point Γ. It should be noted that the peak of the state density in the subband with spin ↑ is located at 0.278 eV according to Batallon's data, and at 0.3 eV according to photoemission data.

In the region of 0.4 eV, a passage through zero and a reversal of sign are observed for all three $\varepsilon_2'(\hbar\omega)^2$ curves. From the point of view of interband transitions, this can be explained as the turning-on, in the subband, transitions with oppositely directed spins. In the considered electronic-structure scheme these transitions are the transitions in the vicinity of the point L, where according to results of the study of the de Haas–van Alphen effect there are hole pockets that intersect in a complicated manner. The singularity in the interband state density, due to the transition $L_2 \rightarrow L_1\downarrow$, is located according to the Batallon's data at an energy 0.46 eV. The connection of transitions in the vicinity of the L point can explain the observed reversal of the sign of the $\varepsilon_2'(\hbar\omega)^2$ curves.

An anisotropic behavior of the $\varepsilon_2'(\hbar\omega)^2$ curves is observed in the energy range 0.5–2.0 eV.

For a sample cut in the basal plane, and for a sample magnetized along the C axis (H ‖ C), it is possible to separate on the $\varepsilon_2'(\hbar\omega)^2$ curves two peaks in the regions of 0.7 and 1.3 eV. When the sample is magnetized along the difficult axis (H ⊥ C) there is no peak in the 0.7 eV region, and the amplitude of the peak in the k, 2 eV region is half as large. This is apparently due to the fact that according to the selection rules for the allowed optical transitions at high-symmetry points of the Brillouin zone in a hexagonal close-packed lattice[18] the transitions depend on the polarization of the vector $\mathbf{E}_p$ of the effective electromagnetic wave at the points Γ, H, K, but not at the points L and M. We therefore identify the transitions in the regions of 0.7 and 1.3 eV with the transitions $\Gamma_3\uparrow \rightarrow \Gamma_5\downarrow$ (for the first peak) and $H_1 \rightarrow H_3\downarrow$, $K_3 \rightarrow K_5\downarrow$ (for the second peak), and these transitions are only partially allowed in the case of magnetization along the difficult axis, when the effective vector $\mathbf{E}_p$ of the electromagnetic wave is directed along the easy axis (E ‖ C). According to Ref. 6, these transitions occur at 0.88, 1.24, and 1.2 eV, respectively.

The singularity at $\hbar\omega = 1.55$ eV, observed for all three curves, can be identified with the transitions $A_3 \rightarrow A_3\downarrow$ and $M_2 \rightarrow M_4\downarrow$, which are allowed for both polarizations of E. The theoretical values for the frequencies of the interband transitions are in this case 1.64 and 1.9 eV, respectively. For energies higher than 2 eV, it is already difficult to speak of individual interband transitions, since at these energies a large number of similar transitions are turned on and it appears that an appreciable contribution can be made also by indirect transitions.

From the foregoing identification it follows that the observed behavior of the magneto-optical properties of Co can be qualitatively explained on the basis of the electronic structure obtained for Co by Batallon and co-workers.[6] The value of the exchange splitting ΔE_{dd} needed to explain the magneto-optical properties agrees with the value ΔE_{dd} that follows from the Stoner–Slater–Wohlfarth ferromagnetism theory. To obtain a more accurate quantitative comparison of the experimental results with the theory it is necessary to calculate all the optical transitions from band to band, as was done by Callaway and Wang[19,20] for nickel and iron.

We are sincerely grateful to I. M. Puzeĭ for supplying the cobalt single crystal.

[1]J. W. Conolly, Phys. Rev. 159, 415 (1967).
[2]S. Wakoh and J. Yamashita, J. Phys. Soc. Jpn. 28, 1151 (1970).
[3]S. Ishida, J. Phys. Soc. Jpn. 33, 369 (1973).
[4]I. Rosenman and F. Batallan, Phys. Rev. 135, 1340 (1972).
[5]P. Heimann, E. Marschall, H. Neddermeyer, M. Pessa, and H. F. Roloff, Phys. Rev. B 16, 2575 (1977).
[6]F. Batallan, I. Rosenman, and C. B. Sommers, Phys. Rev. B 11, 545 (1975).
[7]C. M. Singal and T. P. Das, Phys. Rev. B 16, 5068 (1977).
[8]E. P. Wohlfarth, J. Appl. Phys. 41, 1205 (1970).
[9]A. P. Lenham and D. M. Treherne, in: Optical Properties and Electronic Structure of Metals and Alloys, Amsterdam, 1966, p. 196.
[10]M. M. Kirillova and B. A. Charikov, Opt. Spektrosk. 17, 254 (1964).
[11]L. A. Afanas'eva and M. M. Kirillova, Fiz. Met. Metalloved. 23, 472 (1967).
[12]G. A. Bolotin, M. M. Noskov, and I. I. Sasovskaya, Fiz. Met. Metalloved. 35, 699 (1973).
[13]G. S. Krinchik and V. S. Gushchin, Zh. Eksp. Teor. Fiz. 56, 1833 (1969) [Sov. Phys. JETP 29, 984 (1969)].
[14]G. S. Krinchik and E. A. Gan'shina, Zh. Eksp. Teor. Fiz. 65, 1970 (1973) [Sov. Phys. JETP 38, 983 (1973)].
[15]G. S. Krinchik and G. M. Nurmukhamedov, Zh. Eksp. Teor. Fiz. 48, 34 (1964) [Sov. Phys. JETP 21, 22 (1964)].
[16]I. L. Erskine and E. A. Stern, Phys. Rev. B 8, 1239 (1974).
[17]E. Fawcett and W. A. Reed, Phys. Rev. Lett. 9, 336 (1962).
[18]J. O. Dimmock, A. J. Freeman, and R. E. Watson, in: Optical Properties and Electronic Structure of Metals and Alloys, Amsterdam, 1966, p. 237.
[19]C. S. Wang and J. Callaway, Phys. Rev. B 9, 4897 (1974).
[20]M. Singh, C. S. Wang, and J. Callaway, Phys. Rev. B 11, 287 (1975).

Translated by J. G. Adashko

Unloading isentropes and the equation of state of metals at high energy densities

L. V. Al'tshuler, A. V. Bushman, M. V. Zhernokletov, V. N. Zubarev, A. A. Leont'ev, and V.E. Fortov

All-Union Research Institute of Optical-Physics Measurements
(Submitted 19 July 1979)
Zh. Eksp. Teor. Fiz. 78, 741–760 (February 1980)

The release (unloading) isentropes of shock-compressed samples of copper and lead are experimentally investigated in a wide range of thermodynamic parameters, from states on the shock adiabats (R-H curves) at a pressure 0.5–2.5 Mbar to near-critical states. The investigations make it possible to determine the thermodynamics and to ascertain the form of the phase diagram in this region. An interpolation equation of state is derived to describe the behavior of metals on the entire phase plane, with allowance for high-temperature melting and evaporation. The coefficients of the equations of state are determined and the thermodynamic characteristics of copper and lead are calculated from the results of the experiments and from other experimental and theoretical information.

PACS numbers: 64.30. + t, 65.50. + m

1. INTRODUCTION

The methods developed by now to apply intense pulses on metals (lasers, electron beams, ion and neutron beams, powerful shock and electromagnetic waves[1]) produce in the condensed phase a high local energy concentration exceeding the binding energy, so that a plasma with a strong interparticle interaction is formed. For an adequate description of the physical processes and the motion dynamics in action of this kind it is necessary to know the thermodynamic properties of the material in a wide range of pressures and temperatures, covering the entire spectrum of the states that arise in pulsed energy release. It is particularly important to take a detailed account of the high-temperature melting and evaporation, and to describe correctly the characteristics of the metals under conditions of disorder and great deviation from the ideal state.

An arbitrary phase diagram of a metal is shown in Fig. 1, where the regions that can be treated theoretically and experimentally are marked schematically.

The modern theoretical methods are valid in the limit of extremal high pressures and temperatures, where one can use the quasiclassical (the Thomas–Fermi theory with corrections[2]–TFC) and the classical (the Debye–Huckel[3]) approximations of the self-consistent

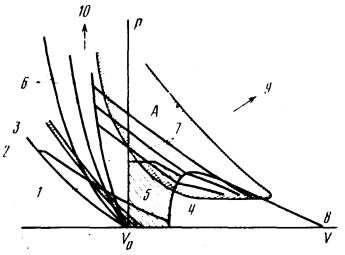

FIG. 1. Arbitrary phase diagram of metal. 1—static experiments, 2—isotherm $T = 293$ K, 3—melting region, 4—liquid–vapor equilibrium curve, 5—exploding-wire method, 6—experimental shock adiabats, 7—release isentropes, 8—ideal gas, 9—ideal plasma, 10—Thomas–Fermi electron gas; A—uninvestigated region with strong interparticle interaction. The arrows point to a decrease of the nonideality parameter.

 0038-5646/80/020373-11$02.40